Article

pubs.acs.org/Biomac

Thermal Expansion of Self-Organized and Shear-Oriented Cellulose Nanocrystal Films

Jairo A. Diaz,*[,†] Xiawa Wu,[‡] Ashlie Martini,[∥] Jeffrey P. Youngblood,[†] and Robert J. Moon[†,⊥,§]

[†]School of Materials Engineering, [‡]School of Mechanical Engineering, and [§]Birck Nanotechnology Center, Purdue University, West Lafayette, Indiana 47907, United States

[∥]School of Mechanical Engineering, University of California, Merced, California 95343, United States

[⊥]Forest Products Laboratory, U.S. Forest Service, One Gifford Pinchot Drive, Madison, Wisconsin 53726, United States

Supporting Information

ABSTRACT: The coefficient of thermal expansion (CTE) of cellulose nanocrystal (CNC) films was characterized using novel experimental techniques complemented by molecular simulations. The characteristic birefringence exhibited by CNC films was utilized to calculate the in-plane CTE of self-organized and shear-oriented self-standing CNC films from room temperature to 100 °C using polarized light image correlation. CNC alignment was estimated via Hermans order parameter (S) from 2D X-ray diffraction measurements. We found that films with no preferential CNC orientation through the thickness (S: ∼ 0.0) exhibited an isotropic CTE (∼25 ppm/K). In contrast, films with aligned CNC orientations (S: ∼0.4 to 0.8) had an anisotropic CTE response: For the highest CNC alignment (S: 0.8), the CTE parallel to CNC alignment was ∼9 ppm/K, while that perpendicular to CNC alignment was ∼158 ppm/K. CNC film thermal expansion was proposed to be due primarily to single crystal expansion and CNC−CNC interfacial motion. The relative contributions of inter- and intracrystal responses to heating were explored using molecular dynamics simulations.

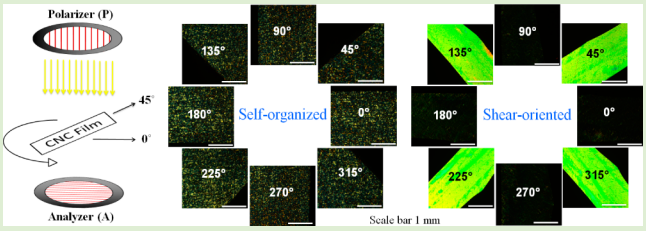

INTRODUCTION

The renewable and sustainable nature of cellulose nanomaterials (CNs) offers a promising alternative to traditional petroleum-based materials in the development of a rapidly growing number of nanotechnology applications in fields such as nanocomposites, organic electronics, and biomaterials.[1−3] CNs are nanoparticles extracted from various cellulose sources (e.g., nonwoody plants, trees, bacteria, algae). Cellulose nanocrystals (CNCs) are one type of cellulose nanoparticle, having a rod-like shape (i.e., 5−20 nm wide by 50−500 nm long) and chemical functionality at the surface (e.g., surface-grafted sulfate half esters) that both affect the ability of CNCs to align by themselves or under the presence of external forces. In CNC composite processing, the orientation of CNCs can be altered in which there is preferential alignment of CNCs in a given direction, which can be achieved by several methods: magnetic fields,[4−9] electric fields,[10−12] mechanical shearing of CNC suspensions,[4,13−16] and combined field and mechanical shearing,[17] CNC composites that have CNC alignment will render different optical, mechanical, and thermal properties that could be tuned according to the application.

The coefficient of thermal expansion (CTE) is important to a variety of fields, for example, electronics where thermal mismatches cause failure of components such as electrodes and composites where thermal mismatches cause dimensional shape changes due to anisotropic CTE and CTE mismatch. Because CNs have been used as substrates for electronics[3,18−20] and as fillers in composites,[1,21] accurate determination of CTE of CNs, CN composites, and the mechanisms for thermal expansion are important, especially with regards to anisotropy and structural organization of the bulk CTE of free-standing films.

The thermal expansion of crystalline cellulose (e.g., Iα, Iβ), and CN composites (e.g., cellulose nanoparticles embedded in a polymer matrix) has been an active area of experimental and modeling research on the crystalline and macroscopic length scales, respectively. The CTE of cellulose Iβ crystals has been experimentally determined at temperatures from −173 to 200 °C based on the d spacing of the (200), (110), (1$\bar{1}$0), and (004) planes and reported to be in the following ranges: 52−136, 40−58, 38−56, and 4−6 ppm/K, respectively.[22−25] Atomistic model-based studies of cellulose Iβ[26,27] predict CTEs in similar ranges yielding values from 25 to 200 °C for the (200), (110), (1$\bar{1}$0), and (004) planes on the order of 90, 65, 67, and 2 ppm/K, respectively. Simulations also reveal a sudden increase in thermal expansion above 200 °C. In composites, the addition of cellulose nanoparticles to a matrix polymer has been shown to lower the macroscopic CTE.[19−21,28−31] In general, the CTE of composite materials depends on the properties of the matrix material (CTE and

Received: June 1, 2013
Revised: July 6, 2013
Published: July 10, 2013

 © 2013 American Chemical Society

stiffness), the polymer, the resulting CN network structure (e.g., percolated vs dispersed), CN-CN bond strength, CN-matrix bond strength, CN volume fraction, and CN alignment.[1] Much of the CNC composite research is focused on the processing and structure property relationships of films.

For measuring the CTE of films, several methods can be used to determine strain as a response to increased temperature (e.g., atomic force microscopy (AFM), Wheatstone half-bridge, thermomechanical analysis (TMA), X-ray diffraction (XRD), bilayer cantilever (BC), interferometry, push-rod dilatometry, etc.). However, only a few techniques are appropriate for CNC films, mostly due to their thickness (~45 μm), thermal variation of stiffness, and hydrophilic nature. Additionally, to use the above-mentioned methods, the specimens have to be permanently in contact with external bodies or one must know the values of certain mechanical properties beforehand (BC method), both of which expose the sample to possible alignment modifications or premature fracture.

To the best of our knowledge, thermal strain has never been measured for CNC films in a contact-free fashion. A contact-free technique is desirable because it can account for the free thermal expansion and interactions of CNCs as well as their resultant effect at larger scales. Any partial or full external contact affects the free expansion of the CNC films (example given herein). Hence, to more accurately determine CTEs, we should isolate the thermal expansion mechanisms from mechanical interactions or other thermally activated processes like creep. Thus, contact free techniques are necessary (e.g., polarized light image correlation (PLIC), electronic speckle pattern interferometry (EPSI), and ellipsometry) for self-standing film testing and future CNC-film-based materials design.

In the current study, digital image correlation (DIC) was used to measure the free thermal expansion of CNC films (in a contact-free manner) as a function of CNC alignment. The CTE was calculated within the plane of the film in the direction parallel to and perpendicular to the CNC alignment direction. The patterning used for DIC was created by the characteristic structural domains within CNC films (e.g., chiral nematic ordering, pitch variations, etc.), as imaged via polarized light microscopy (PLM). To further understand the macroscopic CTE of the neat CNC films, we used molecular dynamics modeling to estimate the relative contributions of both the thermal expansion within a CNC crystal and the CNC−CNC interfacial motion.

EXPERIMENTAL METHODS

Definition of Axes. The following terminology is used to describe the directions within a CNC, between two CNCs, and within the films. This labeling system was chosen to prevent confusion when discussing crystal direction, simulation direction, and CNC film directions. Within the CNC, the cellulose Iβ crystal unit cell directions (i.e., *a*, *b*, *c* axes) and the crystallographic lattice planes (i.e., (200), (110), (1$\bar{1}$0), and (004)) will be used, as defined in Figure 1, where the *c* axis of the crystal is parallel to the cellulose chain axis. When analyzing CNC−CNC interparticle motion, Cartesian directions defined by the simulation are used, which are aligned to the CNCs in a set way. Interparticle behavior is studied using two adjacent CNCs. The *X* axis is parallel to the *c* axis of the "left" cellulose Iβ crystal unit cell. The *Y* axis is perpendicular to the *X* axis and is also parallel to the [1$\bar{1}$0] direction (i.e., expansion between (1$\bar{1}$0) planes). The *Z* axis is defined as being perpendicular to both *X* and *Y* axes. However, because cellulose Iβ has a monoclinic crystal structure, the *Z* axis is ~5° off

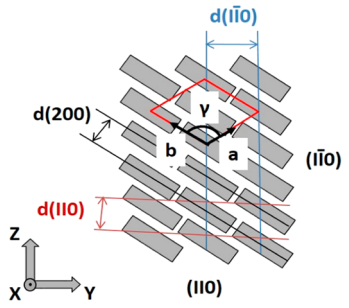

Figure 1. Schematic of an idealized wood CNC cross-section along the cellulose chain-axis direction (i.e., the *c* axis), where each gray box represents a single cellulose chain, showing the terminating surfaces [(110) and (1$\bar{1}$0)] and the Iβ unit cell projection superimposed on the crystal lattice.[1] The *d* spacing of three major lattice planes, (200), (110), and (1$\bar{1}$0), is labeled. The Cartesian coordinates *X*, *Y*, and Z that are used in the simulations for CNC−CNC interaction are also given.

parallel relative to the [110] direction (i.e., the expansion between (110) planes, which results in changes in the "Z" direction).

The directions within the CNC films are defined based on the casting conditions used to make the film (Figure 2). For the films produced without shear, no directionality is defined as self-organized CNCs are considered to be uniformly distributed with no preferred orientation when seen through the film thickness. In contrast, for shear cast films, the directionality is defined with respect to the shear direction, where "axial" is parallel to the shear direction and "transverse" is perpendicular to the shear direction. Whereas these directions are relative to shear rather than the CNCs, previous work has shown that the long axis of the CNC orients in the direction of the shear (i.e., the axial direction of the film). The direction-dependent CTEs of the shear cast CNC films are then defined as CTE_{axial} and CTE_{trans} for measurements parallel to and perpendicular to the shear direction. Finally, for the simulations of the CNC−CNC interparticle motion, the *X* direction is parallel to the "axial" direction of the film.

CNC Film Preparation. Cellulose nanocrystals (CNCs) with 0.81 wt % CNC surface-grafted sulfate content, extracted via sulfuric acid hydrolysis of eucalyptus dry-lap cellulose fibers, were provided by the USDA Forest Service-Forest Products Laboratory, Madison, WI (FPL).[32] Aqueous CNC suspensions with CNC concentrations up to 10.1 wt % were adjusted in pH from 4.4 to 7.2 with 0.2 N NaOH solution to create stable suspensions for film casting. Neat self-organized CNC films (Figure 2a) were produced by pouring ~20 mL of stable CNC suspensions in 8 cm diameter polystyrene Petri dishes and were allowed to evaporate under ambient conditions (23 °C, 35% relative humidity). A testing specimen (SO in the Supporting Information Table S1) with dimensions (~45 μm × 20 mm × 5 mm) was obtained from the middle of the dry circular film to avoid edge defects. Neat CNC films having preferential CNC alignment (A1−A5 in Table S1 in the Supporting Information) were produced in a method similar to that of Reising et al.[16] by shear casting the CNC suspensions on a glass substrate between two 0.6 mm thick polyethylene terephthalate PET strips (Figure 2b). A regular 4 cm wide razor blade was vertically inclined 45° with respect to the substrate to cast in six repetitions 3 mL aliquots of the CNC suspensions at shear rates ranging from 17 to 600 s^{-1} (Table S1 in the Supporting Information). Suspensions employed in the preparation of films A1 and A2 (Table S1 in the Supporting Information) were preheated to 40 °C while stirring for 15 min. After shear casting, all films were allowed to evaporate for 3 days under ambient conditions. Once dry, the CNC films were peeled off from the glass substrate (Figure 2b) and cut into a testing geometry (~45 μm × 20 mm × 5 mm) using a laser cutter (Universal Laser Systems, PLS 3.60).

CNC Alignment Characterization. Self-standing CNC films were evaluated in a Bruker GADDS 2D X-ray diffractometer (2D-XRD) using a 546 nm Cuα source at 40 mA, 20 kV for 600 s and a beam size

dx.doi.org/10.1021/bm400794e | Biomacromolecules 2013, 14, 2900−2908

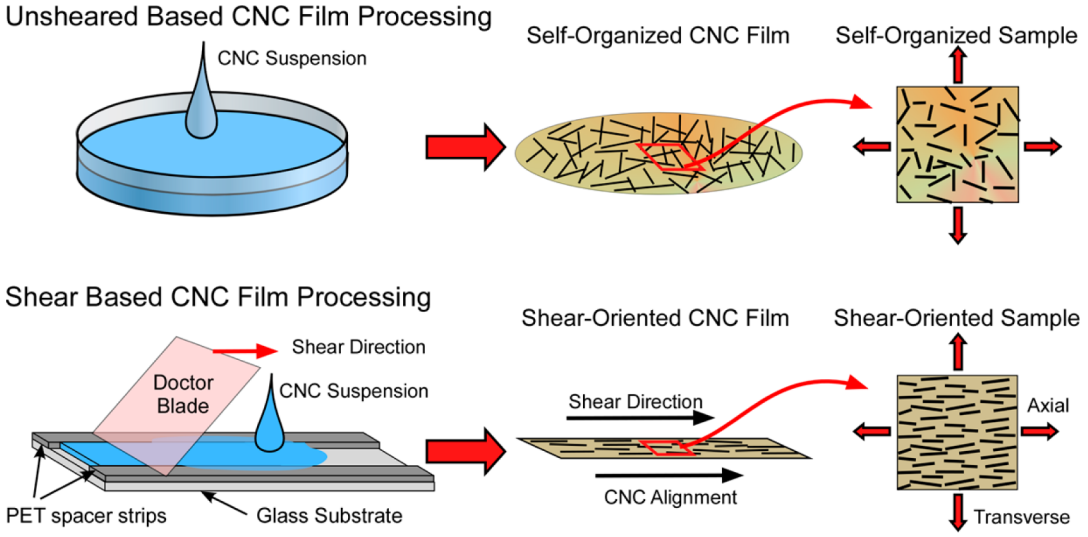

Figure 2. Schematic of CNC film processing and the configuration of the test samples extracted from the as cast films for (a) unsheared and (b) shear casting. The directionality of the shear cast films was defined as "axial" or "transverse" for the direction parallel to or perpendicular to the shear direction.

of 500 μm at 6.1 cm from detector in transmission mode. The Hermans order parameter (S), calculated using eqs 1−3, provided information about the in-plane CNC alignment through the entire film thickness, where S = 0.0 represents no preferential orientation and S = 1.0 represents a fully aligned film.[14] After background subtraction, the integration of the intensity versus azimuthal angle (ϕ) was performed from 0 to 180° around the (200) plane present at 2θ:{21.0−22.3} for cellulose Iβ.

$$S = \frac{3\langle \cos^2 \gamma \rangle - 1}{2} \quad (1)$$

$$\langle \cos^2 \gamma \rangle = 1 - 2\langle \cos^2 \phi \rangle \quad (2)$$

$$\langle \cos^2 \phi \rangle = \frac{\int I(\phi) \cos^2 \phi \sin \phi \, d\phi}{\int I(\phi) \sin \phi \, d\phi} \quad (3)$$

Thermal Expansion Determination in CNC films. The digital image correlation (DIC) methodology used in this study to measure the thermal response of the CNC films consisted of three different stages: image acquisition, image processing, and image correlation. The image acquisition step was performed in a Carl Zeiss (Axio Observer A1) inverted microscope coupled to a heating stage (Linkam PE94), where five different contact-free (36 bit, 2047 pixel × 2047 pixel) images were captured at 25, 40, 60, 80, and 100 °C. A 10 min stabilization time was allowed at each temperature before capturing images. The image processing step was performed in both ImageJ and Adobe Photoshop to adjust each image (e.g., bit transformation, rotations, image contrast, etc.) so that a distinct speckle pattern could be achieved, allowing for precise correlation of pixel intensity among images. The image correlation step was performed in MatLab using the correlation function (cpcorr.m) in the image toolbox and the MatLab open-source files (HighCorr package) designed by R. J. Thompson et al.[33,34]

A speckle pattern in CNC films was generated under crossed polarizers using 5× magnification. Both self-organized and shear-oriented films generated clear patterns employed for image correlation and further calculation of thermal strains, although the nature of the patterns was different due to CNC alignment. To better correlate CNC alignment and thermal expansion of the CNC films, the regions selected for CTE determination via PLIC intended to nearly approach those X-rayed during the CNC orientation calculations. Precision of the method was tested by investigating the influence of number of correlation points and region size/displacement field on the calculated CTE (Figure S1 in the Supporting Information). As the number of correlation points was reduced, the CTE varied by 0.1 ppm/K or less, so it had little effect on the results. CTEs varied by 3 ppm/K or less depending on the analyzed region, indicating small heterogeneities in the film, but maintaining good precision none-the-less.

Modeling and Simulations. Molecular dynamics simulations were used to complement the experimental measurements and provide insight into the molecular scale mechanisms underlying the observed thermal expansion of the CNC films. The specific goals of the modeling effort were to (a) investigate the relative contributions of intra- and intercrystal expansion in multi-CNC systems, (b) determine the limiting behavior for orientation by modeling parallel and perpendicular geometries, and (c) determine if trends in CNC film thermal expansion can be explained or correlated to the thermal response of individual cellulose crystals.

The simulations described either a single cellulose Iβ crystal (Figure 1) or two adjacent cellulose Iβ crystals in parallel and perpendicular configurations (Figure 3a,b). The cellulose Iβ crystal structure was built using Material Studio software with unit cell parameters from X-ray diffraction.[35] The left single crystal consisted of 18 chains and the right consisted of 16 chains, and each molecule chain was treated as a rigid body after equilibration. The sizes of the crystals were 5.40 × 1.99 × 3.37 nm^3 and 4.40 × 1.68 × 3.48 nm^3 for the left and right crystals, respectively. The simulation box had dimensions of 5.40 × 6.00 × 5.40 nm^3. All simulations were run with LAMMPS software with ReaxFF force field, which was validated and used for prediction of cellulose Iβ crystal elasticity previously.[36]

For the CNC−CNC interface models, the "left" crystal (Figure 3a,b) in both systems was modeled to have infinite length in the molecule axial direction by applying a periodic boundary condition in the X direction and a finite cross-sectional area by applying fixed boundary conditions in the transverse directions (i.e., Y and Z directions). The "right" crystal had a finite length and cross-section so that it could move and rotate (within the X−Z plane) due to the intercrystal forces from the "left" crystal. A cellulose Iβ crystal can have six possible terminating surfaces,[37] any two of which can be in contact when two CNCs come in contact with each other. We arbitrarily chose the "right" surface of the "left" crystal to be $(1\bar{1}0)$ and the "left" surface of the "right" crystal to be (200) (Figure 3c). In this study, we focus on the above chosen surfaces, but we do not exclude the possibility that other combinations of contacting surfaces exist in a film.

The single crystals were equilibrated in the NPT ensemble (constant number of atoms, pressure, and temperature) at 27 °C and 1 atm for 50 ps to allow them to reach their stable structures. The two crystal simulation systems were then equilibrated in the NVT ensemble (constant number of atoms, volume, and temperature) at 27

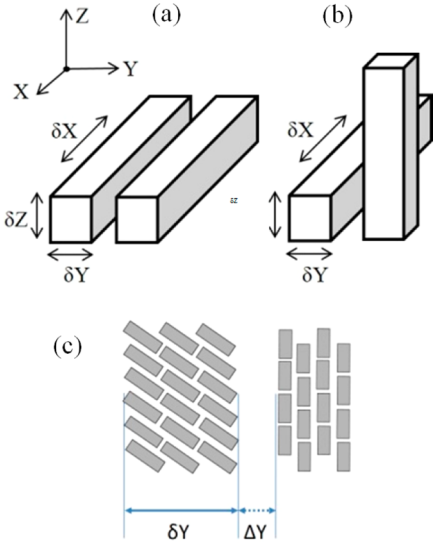

Figure 3. Schematic of the two CNC−CNC configurations: (a) parallel and (b) perpendicular models that were used to investigate CNC−CNC interfacial motion. For each case, the "right" CNC was free to shift in *X*, *Y*, and *Z* directions and rotate within the *Z*−*X* plane. (c) Schematic shows single-crystal thermal expansion (δ) versus intercrystal motion (Δ) in the *Y* direction from the parallel model.

°C for 100 ps and finally heated from 27 to 127 °C for 800 ps. Simulations of both models were repeated four times. The thermal expansion of the single crystals was calculated by identifying the changes of crystal dimensions during the heating process. To validate that the model could accurately predict thermal expansion, we calculated the thermal expansion of the *d* spacing in the left single crystal in both models and found the model predictions were reasonable in the context of experimental measurements. (See the Results and Discussion.) Finally, the movement between the crystals was characterized by the displacement of the center of mass of the right crystal relative to the left crystal in three orthogonal directions. The example in Figure 3c shows the single-crystal thermal expansion (δ) and the intercrystal motion (Δ) in the *Y* direction. Comparing their magnitudes during the same heating conditions will reveal each of their roles in the total thermal expansion. The total thermal expansion was defined as the dimensional changes of the two-crystal model during the heating process and included the effect of the expansion of the two single crystals and their movement relative to one another. The leftmost layer of the "left" crystal was fixed during the entire simulation process to stabilize the system. Note that the *Y* and *Z* directions in the simulation system are collectively comparable to the "transverse" direction in the thin films.

RESULTS AND DISCUSSION

Alignment of CNCs within Films. The dried solution cast CNC films (without shear) exhibited the typical iridescence (Figure 4a), which is associated with chiral nematic organizations,[38] while the shear cast CNC films showed little light interference (Figure 4b). The degree of CNC alignment within these self-standing CNC films was quantified using 2D XRD via Hermans order parameter (*S*).[39] The unsheared CNC film (R in Table S1 in the Supporting Information) exhibited a uniform diffraction pattern (Figure 4c), with uniform intensity at all azimuthal ϕ angles for the (200) 2θ peak, and represents no preferential CNC orientation through the thickness of the film and is confirmed with an $S \approx 0.03$. In contrast, for the shear cast films the (200) planes diffracted more X-rays in the azimuthal ϕ angles perpendicular to the shearing direction than in ϕ angles parallel to the shear direction (Figure 4d) and

Figure 4. (a) Iridescent self-organized CNC film and (b) transparent shear-oriented CNC film. 2D XRD patterns for (c) self-organized CNC film showing uniform intensity "rings" typical of an isotropic response and (d) shear-oriented CNC film, showing anisotropy in the ring intensity.

represent CNC alignment within the film with the CNC long axis orientated parallel to the shear direction. High shear rates during film casting were directly correlated to the highest orientated CNC films (Table S1 in the Supporting Information), whereas lower shear rate, combined with the casting suspension pretreatment just prior to the casting process, produced CNC films (A1 and A2) that had an intermediate CNC alignment.

CTE of Self-Organized CNC Films. CNC films with no preferential CNC orientation through the thickness ($S \approx 0.03$) were analyzed for CTE via PLIC (Figure 5). While such films

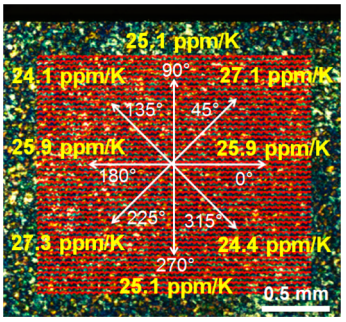

Figure 5. Isotropic in-plane coefficient of thermal expansion of self-organized CNC films.

are conventionally deemed "random" due to the near-zero Hermans order parameter, it must be stated that the CNCs show chiral nematic behavior, and as such, there is local order in the films. However, the domains appear to be arranged randomly within the film so the in-plane properties should be isotropic. The CTE was determined in all directions at 45° angular increments (Figure 5), and as expected, the in-plane thermal expansion was isotropic with a CTE of ~25 ppm/K, which is in between the values of the measured CTEs of the directions of the individual crystals previously found by XRD,[22−25] as summarized in Table 1. In comparison with other materials, self-organized CNC films exhibit significantly lower thermal expansion than other polymeric systems, which typically exhibit CTEs in the 50−200 ppm/K range and are more similar to metals or composites.[1]

To confirm that frictional forces induced by contact can have an effect on CTE values, we also measured the same CNC films while placed between 2 microscope slides. In such a scenario, CTE of the films was ~2 ppm/K, representing more than one order of magnitude decrease. This suggests that contact-based

Table 1. Summary of Thermal Expansion Determination of Cellulose Materials

		CTE (ppm/K)	temp range (°C)	method	ref
Experimental single crystal	**unit cell parameters**				
	a	52−136			
	b	−30 to 21	−173 to 200	XRD	22−25
	c	4−6			
	crystalline planes				
	(200)	52−136			
	(110)	40−58	−173 to 200	XRD	22−25
	$(1\bar{1}0)$	38−56			
	(004)	4−6			
CNC film	**self-organized (SO) *S* = 0.03**				
	axial	25−26	25−100	PLIC	this work
	transverse	25−26			
	shear-oriented (A5) *S* = 0.78				
	axial	9−10	25−100	PLIC	this work
	transverse	154−158			
	extrapolated *S* = 1.0				
	axial	8	25−100	PLIC	this work
	transverse	207			
MD Simulations					
single crystal	**unit cell parameters**[a,b]				
	a	60−104			
	b	27−30	25−200	GROMOS 45a4, GLYCAM06	26, 27
	c	2			
	crystalline planes[a]				
	(200)	56*−90			
	(110)	20*−65	25−200 (27−127)*	GLYCAM06, *ReaxFF	26, *this work
	$(1\bar{1}0)$	19*−67			
	(004)	2			
CNC−CNC interface	**parallel contact**				
	X	9			
	Y	91	27−127	ReaxFF	this work
	Z	187			
	perpendicular contact				
	X	15			
	Y	15	27−127	ReaxFF	this work
	Z	41			

[a]Values taken from ref 26 were estimated from Figure 5. [b]Values taken from ref 27 were estimated from Figure 6.

testing methods may inadvertently involve other contributions stemming from friction or changes in mechanical properties during thermal expansion determination, because of which the sample expansion may be hindered and the CTE underestimated.

CTE of Films with CNC Alignment. The thermal strains as a function of temperature for several films are shown in Figure 6. The nearly linear trends found in the thermal expansion response make the calculated CTEs a reliable representation of the instantaneous thermal strain from room temperature up to 100 °C. The data show that as orientation increases the CTE decreases in the axial (shear) direction, as shown in Figure 6a. In contrast, the thermal expansion in the transverse direction increased markedly with orientation (Figure 6b).

CTE as a function of order parameter shows the effect of increasing CNC alignment on the film CTE and on the anisotropy between CTE_{axial} versus CTE_{trans} (Figure 7). The increasing CTE_{trans} with CNC alignment could be captured by a linear fit ($\{mx + b\}$ where $m = 187.7$, $b = 19.6$) with a goodness of fit of $R^2 = 0.9662$ and 95% confidence bounds. The decrease in CTE_{axial} could be captured using a simple rational fit ($\{a/(x + b)\}$, where $a = 10.76$, $b = 0.3721$) with $R^2 = 0.9947$ and 95% confidence bounds. Figure S3 in the Supporting Information shows PLM images of shear-oriented CNC films employed in CTE calculation via PLIC. Such films exhibit high anisotropy with an anisotropy ratio of >15 at the highest orientation. Films with the highest alignment have a CTE_{axial} similar to ceramics or the lowest CTE metals. Conversely, the CTE_{trans} of the highest orientation films exhibited CTEs more typical of engineering polymers.

Relationship between Thermal Expansion of Single CNCs and CNC films. To identify the origins of the film thermal expansion, the expansion of individual CNC crystals was compared to that of the CNC films. To simplify the comparison between the CTE of films and the CTE of cellulose Iβ, it is desirable to have the CNCs within the films aligned so that the CTE_{axial} and CTE_{trans} have increased association with the cellulose Iβ lattice structure. The special case when $S = 1$ the CNC films can be approximated as individual crystals placed parallel to each other, in which ∼100% of the CNCs would be arranged with the long axis (i.e., *c* axis) aligned parallel to the axial direction of the film (i.e., the shear casting direction in Figure 2). In this configuration, the contribution to the film CTE in the film axial direction from the CNC crystal

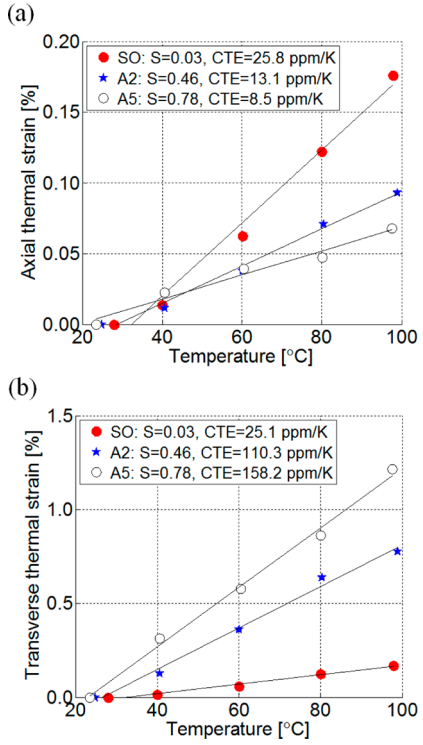

Figure 6. Thermal strain in the axial (a) and transverse (b) directions as a function of temperature for CNC films with different orientations. Behavior exhibited by all tested specimens are included in Figure S2 in the Supporting Information.

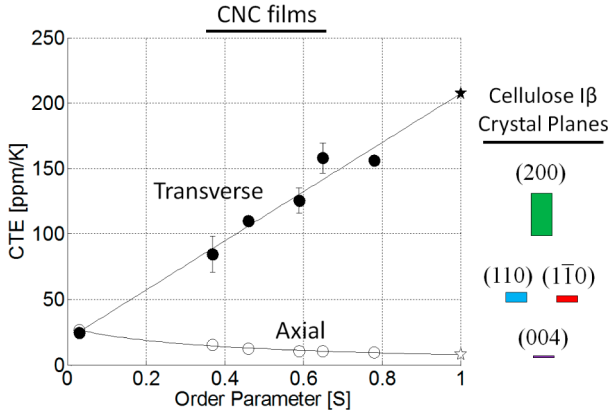

Figure 7. In-plane coefficient of thermal expansion versus Hermans order parameter (S) for CNC films from room temperature to 100 °C, showing how increasing CNC alignment also increases the CTE anisotropy within the films. The trend lines were extrapolated to $S = 1$ for CTE_{trans} (★) and CTE_{axial} (☆) to estimate the CTEs of a hypothetical perfectly aligned film. For comparison with a single cellulose Iβ crystal, the experimental CTEs reported[22−24] for several lattice planes below 200 °C are also given.

would be from expansion in the (004) plane (i.e., in the c axis), whereas in the film transverse direction the CNC particles are free to rotate about their long axis (i.e., c axis) so the contribution to the film CTE would result from the lattice expansions from a distribution of lattice planes (i.e., (110), (1$\bar{1}$0), (200), etc). With this in mind the trend lines for CTE_{axial} and CTE_{trans} were extrapolated to $S = 1$, resulting in 8 and 207 ppm/K, respectively. While these fits are purely arbitrary based on the perceived shape of the data, they do provide the best R^2 values and allow us to cautiously compare with known data of single-crystal CTEs in a very limited fashion. The CTE_{axial} of the most highly aligned CNC films and that of an ideal $S = 1$ CNC film is on the same order as those of a single-crystal c axis obtained from MD and XRD of cellulose Iβ. (See Table 1.) This suggests that the thermal expansion of highly aligned CNC films in the axial direction of the film is dominated by the relatively low CTE of individual CNC crystals in the c axis because either there are negligible contributions from interfacial effects or such effects scale with individual CNC CTE. In contrast, we found that in the transverse direction the CTE of the films was only significantly higher than that from the lattice expansion in the (110), (1$\bar{1}$0), and (200) planes of cellulose Iβ. This indicates that the expansion of the CNC films in the transverse direction cannot be viewed as a simple summation of the expansion of single CNCs. Another means by which films can expand due to heating without (or in addition to) the expansion of individual CNC is through motion between adjacent crystals (i.e., at the CNC−CNC interface). This potential mechanism will be explored in the next section using the molecular simulations.

Molecular Simulations. We first calculated the single-crystal thermal expansion and validated the molecular model by comparing the model-predicted variation of interlayer spacing (d spacing). The CTEs of the lattice planes (200), (110), and (1$\bar{1}$0) simulated in our model were: ∼56, 20, and 19 ppm/K, respectively (Figure 8). The predicted value for the (200) plane

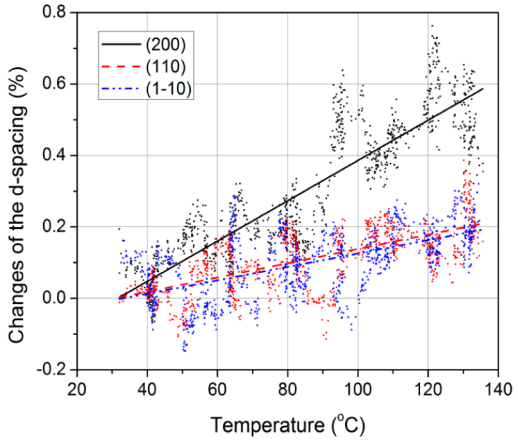

Figure 8. Thermal expansion of three lattice planes (200), (110), and (1$\bar{1}$0) in a single crystal, where $R^2 = 0.77$, 0.45, and 0.35, respectively. An example of expansion from one representative simulation is shown in dots. For each lattice plane, the changes of the d spacing are calculated from the left single crystal in both parallel and perpendicular models and then averaged over four simulations. The lines are linear fits to the data obtained from all simulations, where each simulation data set consists of ∼900 points.

was in the range of experimental results in Table 1, while the values for the (100) and (1$\bar{1}$0) planes were smaller than but still on the same order as the experimental range. This difference may due to the small size of the single crystals in the simulation. The surface molecules of the single crystals are less stable than those inside the crystals, introducing error into the calculation of d spacing changes. Fully atomistic simulations are limited to sizes on the order of a few nanometers because of the significant computational expense associated with the force calculation each time step.

dx.doi.org/10.1021/bm400794e | Biomacromolecules 2013, 14, 2900−2908

Next, we consider the model where two crystals are parallel to one another (Figure 3a). Figure 9 shows both the intracrystal and intercrystal (the "left" crystal only) expansion in response to heating. As shown in Figure 9a, in the X direction (the axial direction of both crystals), the inter- and intracrystal expansions are comparable in magnitude and relatively small. However, as shown in Figure 9b,c, the intercrystal expansion is much more significant than the intracrystal expansion in both the Y and Z directions (transverse). There was no detectable rotation between the two crystals during the heating process.

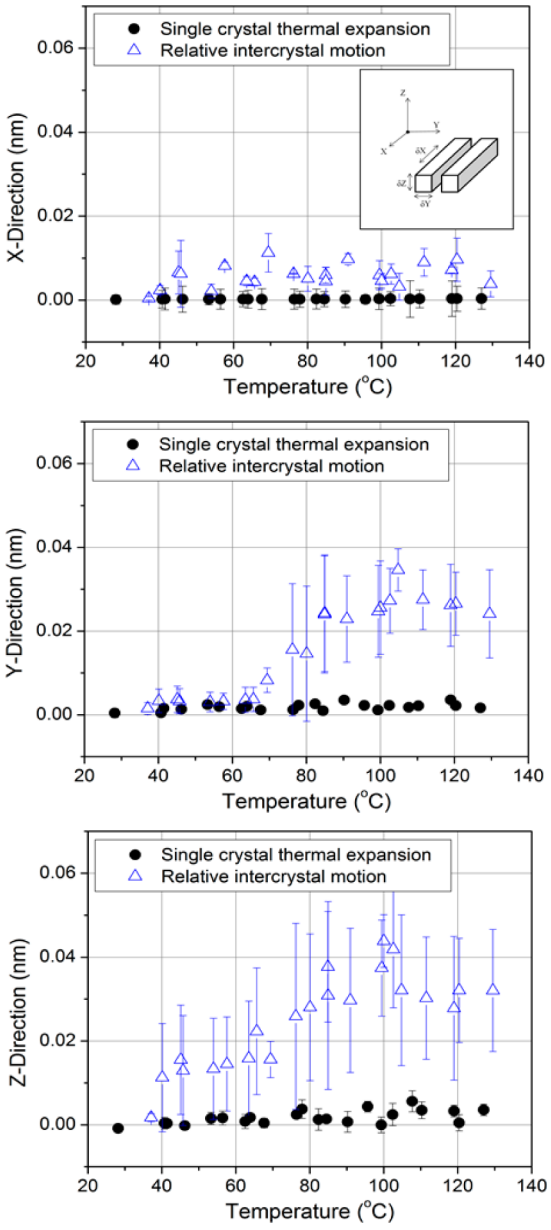

Figure 9. Parallel CNC model response to heating. The single-crystal thermal expansion (circles; δX, δY, δZ) of the "left" crystal and the relative movement between the crystals (triangles; ΔX, ΔY, ΔZ). The values are averaged over four simulations.

For the parallel model, the total expansion in X, Y, and Z directions was $CTE_{\|x} \approx 9$ ppm/K, $CTE_{\|y} \approx 91$ ppm/K, and $CTE_{\|z} \approx 187$ ppm/K, respectively. These values were then compared with the experimental film results extrapolated to $S = 1$ (Figure 7) of $CTE_{axial} \approx 8$ ppm/K and $CTE_{trans} \approx 207$ ppm/K, which bound the range of possible CTEs of the film. The X direction is structurally similar to a perfectly aligned CNC film in the axial direction at $S = 1$, and comparisons show that the model prediction ($CTE_{\|x} \approx 9$ ppm/K) is very close to the experimental film measurement ($CTE_{axial} \approx 8$ ppm/K). The Y and Z directions are more structurally similar to the transverse direction of the perfectly aligned crystal assembly film at $S = 1$, and comparisons show that model predictions ($CTE_{\|y} \approx 91$ ppm/K and $CTE_{\|z} \approx 187$ ppm/K) are similar to the experimental film measurements ($CTE_{trans} \approx 207$ ppm/K). The model predicts that the CNC−CNC intercrystal motion is more significant in the transverse directions than in the axial direction. This significant amount of intercrystal motion in the transverse directions may partially explain the discrepancy between the CTE of the experimental film in the transverse direction ($CTE_{trans} \approx 207$ ppm/K) and the experimental single-crystal lattice expansion for (200), (110), ($1\bar{1}0$), as shown in Figure 7.

A perpendicular model (Figure 3b) was developed to establish if differences in angle between individual CNC crystals can have an effect on the CNC−CNC intercrystal motion. It must be stated that this arrangement does not represent the unsheared case, as self-organized CNC films have a chiral nematic structure. The perpendicular state likely represents one limit for intercrystal expansion, while the parallel case represents the other, and thus taken together they can help bound the relative motion between crystals. However, it cannot be discounted that the perpendicular state does not exist in lower orientation films as intermediate orientations exist somewhere between chiral nematic and parallel. The simulation results for the perpendicular model are shown in Figure 10. In all three directions, X, Y, and Z, the expansion of the single crystals was comparable in magnitude to the relative movement between crystals. This model also exhibited some rotation between the two crystals in the X−Z plane. However, the maximum rotation was less than 2°, and the time-averaged rotation was negligible, so rotational contributions to the results are considered to be minimal. In the perpendicular model, the CTEs of the model total expansion in the X, Y, and Z directions were: $CTE_{\perp x} \approx 15$ ppm/K, $CTE_{\perp y} \approx 41$ ppm/K, and $CTE_{\perp z} \approx 15$ ppm/K. These values are more similar to each other than those in the parallel model.

Considering both the parallel and perpendicular models, we can see that the CNC−CNC interface can produce a mechanism for relative thermal movement, which is related to the contact configuration between CNCs (i.e., parallel vs perpendicular). The relative intercrystal motion in the Y and Z directions was greater when the CNC−CNCs were stacked in parallel as opposed to perpendicular. For the parallel CNC−CNC interface configuration, the relative intercrystal motion was greater than that of the CNC crystal expansion and thus may play a role in the macroscopic CTE behavior of CNC films. Thus, the relative movement between crystals may fill the gap between the thermal expansion of the single crystals and the bulk CNC films.

CONCLUSIONS

We were able to explore the influence of CNC orientation on the in-plane thermal expansion of neat CNC films in a contact-free way via PLIC utilizing the distinct birefringent optical properties of CNC films. Oriented CNC films exhibited a highly anisotropic in-plane thermal expansion as compared with the isotropic response determined in self-organized films. As

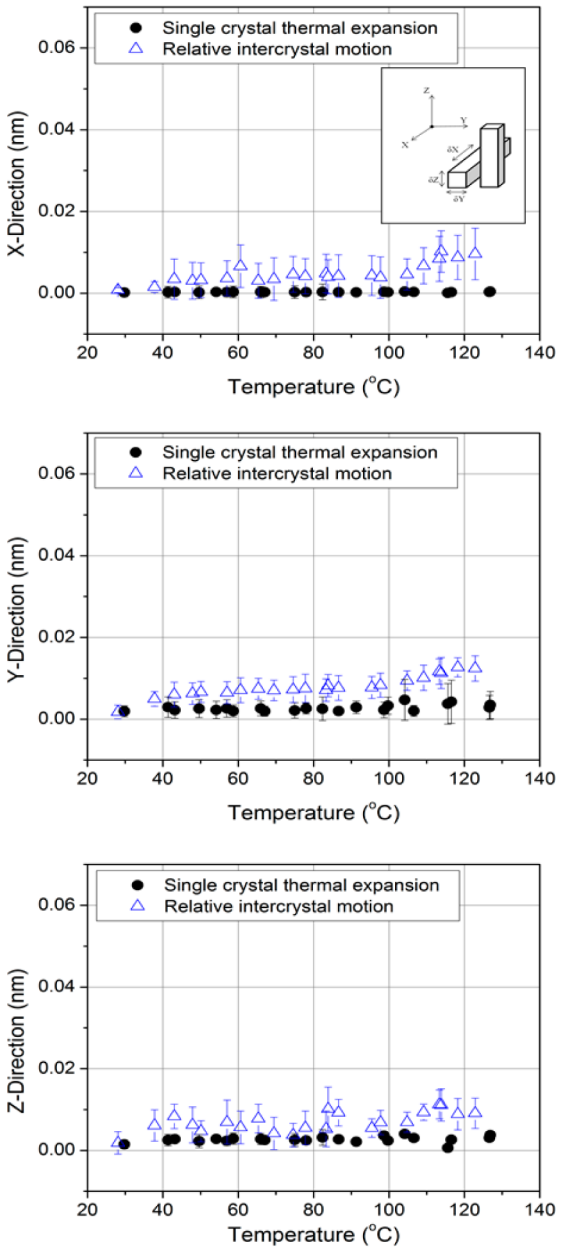

Figure 10. Perpendicular CNC model response to heating. The single-crystal thermal expansion (circles; δX, δY, δZ) of the "left" crystal and the relative movement between the crystals (triangles; ΔX, ΔY, ΔZ). The values are averaged over four simulations.

the Hermans order parameter increased in CNC films, the axial CTE decreased to be on the order of that of ceramics (~10 ppm/K), whereas the CTE in the transverse direction approximates to that of polymers (>50 ppm/K). Simulation results suggested a temperature-induced motion between crystals (i.e., CNC−CNC interfacial motion) that contributes to thermal expansion of CNC films.

■ ASSOCIATED CONTENT

Ⓢ Supporting Information

Table with shear rates employed during tape casting and Hermans order parameters for tested CNC films. Figure containing adjustment of CTE measurement conditions for tested CNC films. Plots of axial and transverse strains versus temperature for all tested specimens. PLM images of shear-oriented CNC films employed in CTE calculation via PLIC. This material is available free of charge via the Internet at http://pubs.acs.org.

■ AUTHOR INFORMATION

Corresponding Author

*E-mail: jdiazama@purdue.edu. Tel: +1 405-3109811.

Author Contributions

The manuscript was written through contributions of all authors.

Notes

The authors declare no competing financial interest.

■ ACKNOWLEDGMENTS

We thank the Air Force Office of Scientific Research grant #FA9550-11-1-0162 for supporting this project.

■ REFERENCES

(1) Moon, R. J.; Martini, A.; Nairn, J.; Simonsen, J.; Youngblood, J. *Chem. Soc. Rev.* **2011**, *40*, 3941−3994.
(2) Habibi, Y.; Lucia, L. A.; Rojas, O. J. *Chem. Rev.* **2010**, *110*, 3479−3500.
(3) Zhou, Y.; Fuentes-Hernandez, C.; Khan, T. M.; Liu, J.-C.; Hsu, J.; Shim, J. W.; Dindar, A.; Youngblood, J. P.; Moon, R. J.; Kippelen, B. *Sci. Rep.* **2013**, *3*, 1536.
(4) Orts, W. J.; Godbout, L.; Marchessault, R. H.; Revol, J.-F. *Macromolecules* **1998**, *31*, 5717−5725.
(5) Kvien, I.; Oksman, K. *Appl. Phys. A: Mater. Sci. Process.* **2007**, *87*, 641−643.
(6) Cranston, E. D.; Gray, D. G. *Sci. Technol. Adv. Mater.* **2006**, *7*, 319−321.
(7) Revol, J. F.; Godbout, L.; Dong, X. M.; Gray, D. G.; Chanzy, H.; Maret, G. *Liq. Cryst.* **1994**, *16*, 127−134.
(8) Kimura, F.; Kimura, T.; Tamura, M.; Hirai, A.; Ikuno, M.; Horii, F. *Langmuir* **2005**, *21*, 2034−2037.
(9) Sugiyama, J.; Chanzy, H.; Maret, G. *Macromolecules* **1992**, *25*, 4232−4234.
(10) Habibi, Y.; Heim, T.; Douillard, R. *J. Polym. Sci., Part B: Polym. Phys.* **2008**, *46*, 1430−1436.
(11) Bordel, D.; Putaux, J. L.; Heux, L. *Langmuir* **2006**, *22*, 4899−4901.
(12) Gindl, W.; Emsenhuber, G.; Maier, G.; Keckes, J. *Biomacromolecules* **2009**, *10*, 1315−1318.
(13) Ebeling, T.; Paillet, M.; Borsali, R.; Diat, O.; Dufresne, A.; Cavaille, J. Y.; Chanzy, H. *Langmuir* **1999**, *15*, 6123−6126.
(14) Nishiyama, Y.; Shigenori, K.; Masahisa, W.; Takeshi, O. *Macromolecules* **1997**, *30*, 6395−6397.
(15) Hoeger, I.; Rojas, O. J.; Efimenko, K.; Velev, O. D.; Kelley, S. S. *Soft Matter* **2011**, *7*, 1957−1967.
(16) Reising, A. B.; Moon, R. J.; Youngblood, J. P. *J. Sci. Technol. For. Prod. Processes* **2013**, *2*, 32−41.
(17) Csoka, L.; Hoeger, I. C.; Peralta, P.; Peszlen, I.; Rojas, O. J. *J. Colloid Interface Sci.* **2011**, *363*, 206−212.
(18) Nakagaito, A. N.; Nogi, M.; Yano, H. *MRS Bull.* **2010**, *35*, 214−218.
(19) Nogi, M.; Yano, H. *Adv. Mater. Commun.* **2008**, *20*, 1849−1852.
(20) Okahisa, Y.; Yoshida, A.; Miyaguchi, S.; Yano, H. *Compos. Sci. Technol.* **2009**, *69*, 1958−1961.
(21) Nakagaito, A. N.; Yano, H. *Cellulose* **2008**, *15*, 555−559.
(22) Wada, M. *J. Polym. Sci., Part B: Polym. Phys.* **2002**, *40*, 1095−1102.
(23) Wada, M.; Hori, R.; Kim, U.-J.; Sasaki, S. *Polym. Degrad. Stab.* **2010**, *95*, 1330−1334.
(24) Hori, R.; Wada, M. *Cellulose* **2005**, *12*, 479−484.
(25) Hidaka, H.; Kim, U.-J.; Wada, M. *Holzforschung* **2010**, *64*, 167−171.

(26) Zhang, Q.; Bulone, V.; Ågren, H.; Tu, Y. *Cellulose* **2011**, *18*, 207−221.
(27) Bergenstråhle, M.; Berglund, L. A.; Mazeau, K. *J. Phys. Chem. B* **2007**, *111*, 9138−9145.
(28) Iwamoto, S.; Nakagaito, A. N.; Yano, H.; Nogi, M. *Appl. Phys. A: Mater. Sci. Process* **2005**, *81*, 1109−1112.
(29) Nogi, M.; Abe, K.; Handa, K.; Nakatsubo, F.; Ifuku, S.; Yano, H. *Appl. Phys. Lett.* **2006**, *89*, 233123.
(30) Ifuku, S.; Nogi, M.; Abe, K.; Handa, K.; Nakatsubo, F.; Yano, H. *Biomacromolecules* **2007**, *8*, 1973−1978.
(31) Shimazaki, Y.; Miyazaki, Y.; Takezawa, Y.; Nogi, M.; Abe, K.; Ifuku, S.; Yano, H. *Biomacromolecules Notes* **2007**, *8*, 2976−2978.
(32) http://www.fpl.fs.fed.us/research/facilities/nanocellulose_pilot-plant.php (accessed May 27, 2013).
(33) http://www.mathworks.com/matlabcentral/fileexchange (accessed October 15, 2012).
(34) Thompson, R.; Hemker, K. *Proc. SEM Conf. Exp. Mech.* **2007**, *2*, 1058−1067.
(35) Nishiyama, Y.; Langan, P.; Chanzy, H. *J. Am. Chem. Soc.* **2002**, *124*, 9074−9082.
(36) Wu, X.; Moon, R. J.; Martini, A. *Cellulose* **2013**, *20*, 43−55.
(37) Ding, S.-Y.; Himmel, M. E. *J. Agric. Food Chem.* **2006**, *54*, 597−606.
(38) Majoinen, J.; Kontturi, E.; Ikkala, O.; Gray, D. G. *Cellulose* **2012**, *19*, 1599−1605.
(39) Ureña-Benavides, E. E.; Kitchens, C. L. *Macromolecules* **2011**, *44*, 3478−3484.